Relativistic effects on the optical response of InSb by time-dependent density-functional theory

Kootstra, F.; de Boeij, P. L.; Aissa, H.; Snijders, J. G.

Published in:
Journal of Chemical Physics

DOI:
10.1063/1.1334615

Publication date:
2001

Relativistic effects on the optical response of InSb by time-dependent density-functional theory

F. Kootstra,[a] P. L. de Boeij, H. Aissa, and J. G. Snijders
Theoretical Chemistry, Materials Science Centre, Rijksuniversiteit Groningen, Nijenborgh 4, 9747 AG Groningen, The Netherlands

(Received 5 October 2000; accepted 1 November 2000)

In this paper we show how relativistic effects can be included in the time-dependent density-functional theory (DFT) for the optical response properties of nonmetallic crystals. The dominant scalar relativistic effects have been included using the zeroth-order regular approximation (ZORA) in the ground-state DFT calculations, as well as in the time-dependent response calculations. We show that this theory can also be applied to indium antimonide in the zinc-blende structure, notwithstanding the fact that it turns into a semimetal when scalar relativistic effects are included. Results are given for the band structure, the static dielectric constant ϵ_∞ and the dielectric function $\epsilon(\omega)$, for the various levels on which relativity can be included, i.e., nonrelativistic, only in the ground-state, or also in the response calculation. Comparisons of our calculated results are made with experiment and other theoretical investigations. With the inclusion of scalar relativistic effects, the band structure of InSb becomes semimetallic within the local density approximation and we find a deviation of 5% from experiment for the static dielectric constant. Also the dielectric function is improved and the spectra are in good agreement with experiment, although the spectral features are shifted to somewhat lower energies compared to experiment. © *2001 American Institute of Physics.* [DOI: 10.1063/1.1334615]

I. INTRODUCTION

In a recent paper[1] we found that time-dependent density-functional theory (TDDFT)[2] in the adiabatic local density approximation (ALDA) works very well for a large range of nonmetallic crystals, for which we achieved, on average, an accuracy of about 5% compared with experiment. A clear exception, however, was found for InSb in the zinc-blende structure ($a=6.48$ Å), for which the predicted static dielectric constant was underestimated by about 40% compared with experiment.[3] Simultaneously we found a considerable overestimation of the experimental band gap, 0.99 eV DFT-LDA, in comparison with experimental band gaps of 0.17 eV[4] ($T=300$ K) and 0.23 eV[5] ($T=0$ K) for this small-gap semiconductor. This overestimation of the band gap is in clear contrast with the general trend which is observed in LDA band structure calculations, i.e., that the band gaps are generally underestimated by about 50%. The inclusion of scalar relativistic effects within the zeroth-order regular approximation in our full-potential ground-state DFT-LDA band structure calculation causes the lowest *s*-like conduction band to be stabilized considerably more than the upper *p*-like valence bands. The band order is changed in the center of the Brillioun zone (BZ), which results in a vanishing band gap, and consequently the incorrect prediction of the InSb crystal being a semimetal. A simular result was found in the fully relativistic linear-muffin-tin-orbital method (LMTO) of Cardona *et al.*[6] and in the full-potential scalar relativistic linear augmented plane-wave (FLAPW) calculation of Guo *et al.*[7] In this paper we investigate the effects on the optical response properties of InSb after including scalar relativistic ZORA in the ground-state DFT, as well as in the time-dependent response calculations. The outline of this paper is as follows. First we show the way in which scalar relativistic ZORA is incorporated in the present TDDFT calculations, and validate the use of the TDDFT equations in this special case of semimetallic InSb. This is followed by a section about the method and implementation. Then, in the next section, we present the results for the band structure, the dielectric constant and function for InSb, and compare these with experimental data. Finally, in the last section, we draw the conclusions.

II. THEORY

Scalar relativistic (SR) effects can be included in the ground-state DFT calculation as described by van Lenthe *et al.* in Refs. 8 and 9 and Philipsen *et al.* in Ref. 10, by replacing the kinetic-energy operator by the ZORA term

$$T_{\mathrm{ZORA}}^{\mathrm{SR}} = p \cdot \frac{c^2}{2c^2 - v_{\mathrm{eff}}(\mathbf{r})} p, \tag{1}$$

in which $p=-i\nabla$, c the velocity of light, and $v_{\mathrm{eff}}(\mathbf{r})$ the self-consistent effective potential. This results in a semimetallic band structure for InSb, the bottom *s*-like conduction band is lowered in energy, below the top *p*-like valence band in the center of the BZ. The Fermi energy coincides with the three degenerate energy bands of *p*-character at Γ. Two of these are completely occupied and one is unoccupied, hence there is no Kohn–Sham band gap. However, the Fermi-surface reduces to a point (Γ), and more importantly, the

[a]Electronic mail: F.KOOTSTRA@CHEM.RUG.NL

density of states vanishes at the Fermi energy. In this special case we expect no intraband contributions so we can use our TDDFT formulas[1] as before. The susceptibility of this isotropic material follows as one-third of the trace of the susceptibility tensor according to[2]

$$\chi_e(\omega)=\frac{1}{3}\sum_i \left\{ \frac{-1}{\omega^2 V}[\delta \mathbf{J}_p(\omega)-\delta \mathbf{J}_p(0)]_i \Big|_{\mathbf{E}=-i\omega \mathbf{e}_i} \right\}, \tag{2}$$

in which the macroscopic paramagnetic current $\delta \mathbf{J}_p(\omega)$ that is induced by a macroscopic electric field $\mathbf{E}(\omega)$ is obtained from

$$\delta \mathbf{J}_p(\omega)=\int\int \left(\frac{i}{\omega}\chi_{\mathbf{jj}}(\mathbf{r},\mathbf{r}',\omega)\cdot \mathbf{E}_{\mathrm{mac}}(\omega) + \chi_{\mathbf{j}\rho}(\mathbf{r},\mathbf{r}',\omega)\,\delta v_{\mathrm{eff}}(\mathbf{r}',\omega) \right) d\mathbf{r}'\,d\mathbf{r}. \tag{3}$$

Here the induced effective potential $\delta v_{\mathrm{eff}}(\mathbf{r}',\omega)$ is lattice periodic and comprises the induced microscopic part of the Coulomb and exchange-correlation contributions. It is a functional of the induced density and in linear response it can be given in the adiabatic approximation by

$$\delta v_{\mathrm{eff}}(\mathbf{r},\omega)=\int \frac{\partial v_{\mathrm{eff}}[\rho](\mathbf{r})}{\partial \rho(\mathbf{r}')}\delta\rho(\mathbf{r}',\omega)\,d\mathbf{r}', \tag{4}$$

where the ground-state expression is used for the functional dependence of the $v_{\mathrm{eff}}[\rho](\mathbf{r})$. The induced density is obtained by solving the following equation self-consistently:

$$\delta\rho(\mathbf{r},\omega)=\int \left(\frac{i}{\omega}\chi_{\rho\mathbf{j}}(\mathbf{r},\mathbf{r}',\omega)\cdot \mathbf{E}_{\mathrm{mac}}(\omega) + \chi_{\rho\rho}(\mathbf{r},\mathbf{r}',\omega)\,\delta v_{\mathrm{eff}}(\mathbf{r}',\omega) \right) d\mathbf{r}'. \tag{5}$$

In these equations the various response kernels follow from the expression

$$\chi_{ab}(\mathbf{r},\mathbf{r}',\omega) = \frac{V}{4\pi^3}\sum_{i,a}\int \frac{(\psi^*_{i\mathbf{k}}(\mathbf{r})\hat{a}\,\psi_{a\mathbf{k}}(\mathbf{r}))(\psi^*_{a\mathbf{k}}(\mathbf{r}')\hat{b}\,\psi_{i\mathbf{k}}(\mathbf{r}'))}{\epsilon_{i\mathbf{k}}-\epsilon_{a\mathbf{k}}+\omega+i\eta}d\mathbf{k} + \mathrm{c.c.}(-\omega), \tag{6}$$

in which i runs over all occupied and a over all virtual band indices. The operator $\hat{a}$ and $\hat{b}$ are either the density or the current operator. The acronym c.c.$(-\omega)$ denotes the complex conjugate expression at negative frequency. The Bloch functions $\psi_{n\mathbf{k}}(\mathbf{r})$ are the solutions of the ground-state ZORA equation with eigenvalues $\epsilon_{n\mathbf{k}}$

$$\left[-\nabla\cdot\frac{c^2}{2c^2-v_{\mathrm{eff}}(\mathbf{r})}\nabla + v_{\mathrm{eff}}(\mathbf{r}) \right]\psi_{n\mathbf{k}}(\mathbf{r})=\epsilon_{n\mathbf{k}}\psi_{n\mathbf{k}}(\mathbf{r}). \tag{7}$$

The four appearing kernels are obtained by substituting for $\hat{a}$ and $\hat{b}$ either $\hat{\rho}=1$ or the relativistic velocity operator $\hat{\mathbf{j}}$, which is given by

$$\hat{\mathbf{j}}=-i[\mathbf{r},\hat{\mathcal{H}}_{\mathrm{ZORA}}]=-i\frac{c^2}{2c^2-v_{\mathrm{eff}}(\mathbf{r})}\nabla+\mathrm{h.a.}, \tag{8}$$

where h.a. is the Hermitian adjoint expression. As can be seen by inspecting Eqs. (3) and (5), the factors involving the operator $\hat{\mathbf{j}}$ are always integrated, so that only the values of the matrix elements matter. The absence of an energy gap, and the quadratic dispersion of the valence and conduction bands make it necessary to investigate the small-frequency behavior of the response kernels. In the Appendix we show that all off-diagonal matrix elements are of the order $\mathcal{O}(|\mathbf{k}|^2)$, thus falling-off sufficiently fast to smooth any singular behavior near $\omega=0$, such that the electrical susceptibility has the asymptotic behavior $\chi_e(\omega)\approx\chi_e(0)+\mathcal{O}(\sqrt{\omega})$.

III. METHOD AND IMPLEMENTATION

The ground-state DFT calculations are performed by using the Amsterdam Density Functional BAND-structure program (ADF-BAND).[11,12] The general characteristics of this implementation are described in Ref. 1 and more specific details can be found, e.g., about the accurate numerical integration scheme, for evaluating matrix elements between basisfunctions which are either numerical atomic orbitals (NAO) or Slater type exponential functions (STO) in Refs. 11 and 13, the density fitting procedure, for evaluating the Coulomb potential, in Ref. 14, and the quadratic tetrahedron method, for evaluating the integrals over the BZ, in Refs. 15 and 16. In the time-dependent extension[2] on this DFT implementation we employ a lattice periodic (microscopic) effective scalar potential, in combination with a uniform (macroscopic) transverse electric field $\mathbf{E}_{\mathrm{mac}}(\mathbf{r},t)$. For solving the TDDFT equations, an iterative scheme is used, with a fixed macroscopic electric field and in which the microscopic potential is updated in each cycle, until self-consistency in the first order density change $[\delta\rho(\mathbf{r},\omega)]$ is established. The evaluation of the integrals over the irreducible Brillouin zone (IBZ) in the Kohn–Sham response kernels, $\chi_{ab}(\mathbf{r},\mathbf{r}',\omega)$ (which show up in the first order density change) are done numerically with integration weights as described in Ref. 1, so singularities in the response kernels, at resonance frequencies, are handled analytically. Finally, after establishing self-consistency in the density change, we obtain the electric susceptibility $\chi_e(\omega)$ and thus the dielectric function $\epsilon(\omega)$ from the (paramagnetic) induced current $\delta\mathbf{j}_p(\mathbf{r},\omega)$, hereby using the conductivity sum rule. Results for the dielectric function of various nonmetallic crystals using this TDDFT implementation can be found in Ref. 1.

IV. RESULTS FOR INDIUM ANTIMONIDE

A. Band structure

In Fig. 1 we show the band structure of InSb, with and without the inclusion of scalar relativistic effects in the ground-state DFT calculation. In order to facilitate the comparison between the two band structure calculations we made the Fermi energy levels coincide. The calculations were done by using a 3Z2P NAO/STO basis (basis V in the BAND program), which is a triple zeta basis augmented with two

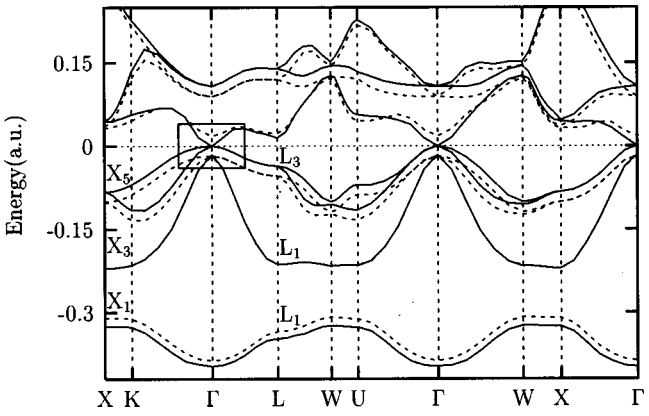

FIG. 1. Band structure of indium antimonide (InSb), the solid line is the scalar relativistic (SR), and the dashed line is the nonrelativistic (NR) ground-state calculation.

polarization functions and frozen core. In the calculations, the $4d$ atomic states of In and Sb were included in the valence basis. These states give rise to shallow core bands, which can affect the position of the valence band maximum.[6,7] As can be seen from the band structure in Fig. 1 and the blowup of the band structure around the center (Γ) of the BZ in Fig. 2, the inclusion of scalar relativistic effects stabilizes the lowest *s*-like conduction band considerably more than the highest valence bands.[17,18] Consequently the conduction band is lowered in energy below the top valence bands, and this causes an avoided crossing between the *s*-like conduction band and one of the valence bands. These bands change in character from *s*-like to *p*-like near Γ and vice versa, as indicated in Fig. 2. The ordering of the energy bands is changed and the bandgap vanishes at the Γ point. Thus LDA-ZORA predicts InSb to be a semimetal, as was also found in Ref. 19 and in the full-potential scalar relativistic LAPW calculations of Ref. 7. The inclusion of spin–orbit coupling in the relativistic calculation will only cause a splitting of the top *p*-like valence bands into an occupied $p_{1/2}$ band and a half occupied $p_{3/2}$ band, thereby leaving InSb to be a semimetal, as was confirmed by earlier fully relativistic LMTO calculations in Ref. 6. Experimentally InSb is found to be a semiconductor with a narrow bandgap of 0.23 eV.[5] In

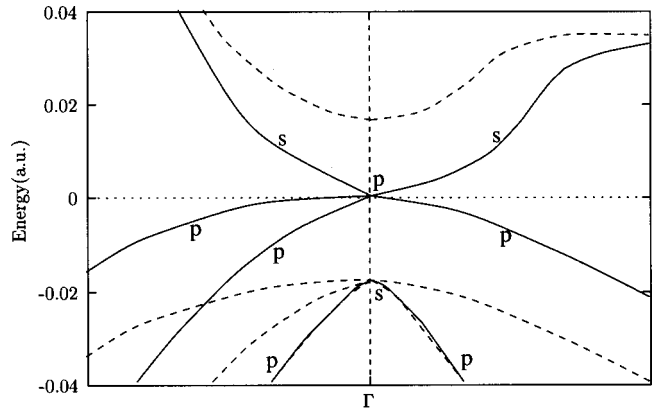

FIG. 2. Blowup of the band structure around the center (Γ) of the Brillioun zone, as indicated in Fig. 1. The solid line is the SR and the dashed line is the NR ground-state calculation.

TABLE I. Static dielectric constant of InSb including non/scalar relativistic (NR/SR) effects in the ground-state/time-dependent DFT calculation, and error compared to the experimental value of 15.7 [E. Burstein, H. Brodsky, and G. Lucousky, Int. J. Quantum Chem. **1**, 756 (1967)].

k-space/ # **k**-points	NR/NR	Error (%)	SR/NR	Error (%)	SR/SR	Error (%)
3/15	11.91	24	18.13	15	18.12	15
4/34	11.22	29	16.63	6	16.61	6
5/65	9.15	42	16.91	8	16.42	5

our SR band structure we find the generally accepted trend for DFT-LDA band structure calculations, that the band gaps are normally underestimated for semiconductors, and in the case of InSb predicting this crystal even to be a semimetal. Nevertheless the scalar relativistic calculated band structure is in good agreement with experiment,[20] e.g., comparing the valence band width of 10.8 eV in our SR band structure with experiment[20] of 11.2 eV [ultraviolet photoemission spectroscopy (UPS)] and 11.7 eV [x-ray photoemission spectroscopy (XPS)]. The valence band energies for L_3, X_3, and X_1 [see Fig. 1] are -1.0, -6.0, and -8.8 eV, respectively, which is also in good agreement with the UPS experimental values of -1.1, -6.5, and -9.0 eV, respectively.

B. Static dielectric constant

In Table I we give the values for the calculated static dielectric constant (ϵ_∞) for InSb with and without including scalar relativistic effects in the ground-state and also the time-dependent DFT calculation. For the integration in reciprocal space we used several accuracies, in which we varied the number of **k**-points in the irreducible part of the Brillouin zone (IBZ). The improvement upon the static value for the dielectric constant with the inclusion of SR effects in the ground-state DFT calculation is very clear from Table I. Looking at the relative errors compared to the experimental value ($\epsilon_\infty = 15.7$) of Ref. 3, it can be seen that the error is 42% in the nonrelativistic calculation, and 8% when scalar relativistic effects were included in the ground-state calculation. From Table I it can be seen that for the value of ϵ_∞ the inclusion of SR effects in the ground-state DFT calculation is most significant, and that the improvement becomes even more evident when SR effects are also included in the response calculation. Now, after including SR effects for InSb, we find the same accuracy for ϵ_∞, about 5% deviation from experiment, as we found earlier for the III-V compounds in the zinc-blende structure of Ref. 1. Other theoretical calculations for the ϵ_∞ of InSb by Huang *et al.*[21] were less accurate, their value of 13.51 underestimates experiment[3] by 14%. This nonrelativistic value was obtained from an uncoupled response calculation in which the χ_0 response is directly calculated from the ground-state DFT solutions, and therefore, this value does not include the Coulomb or exchange-correlation contributions.

C. Dielectric function

In Fig. 3 we show the dielectric function $\epsilon(\omega)$ of InSb, with and without the inclusion of scalar relativistic effects in

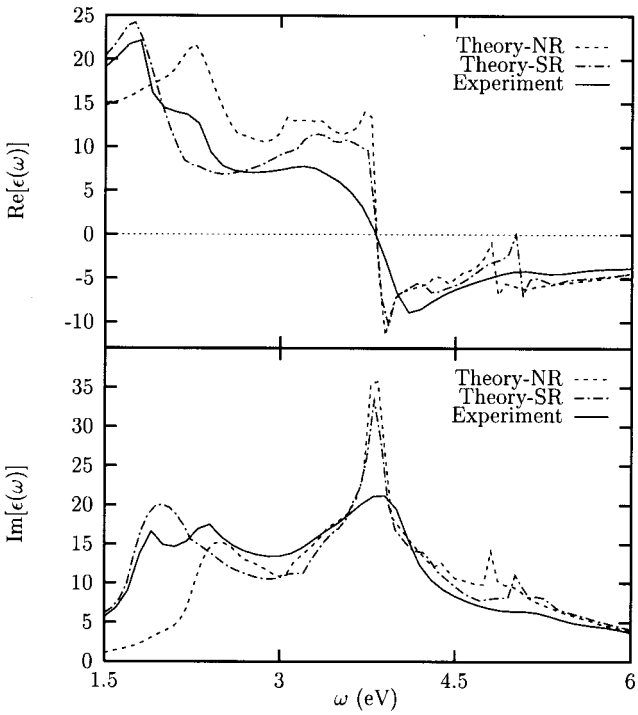

FIG. 3. Plots of the real and imaginary part of the calculated dielectric function of InSb including nonscalar relativistic (NR/SR) effects in the ground-state/time-dependent DFT calculation, in comparison with the experimental data [P. E. Aspnes and A. A. Studna, Phys. Rev. B **27**, 985 (1983)]. The calculated spectra are shifted 0.15 eV NR, and 0.3 eV in the SR case.

the ground-state DFT calculation, in comparison with the experimental data of Ref. 22. The result for $\epsilon(\omega)$ with SR effects also included in the response calculation did not deviate by more than a few percent from the one in which SR effects were only included in the ground-state calculation. The calculated spectra for $\epsilon(\omega)$ were shifted to higher energies in order to facilitate the comparison with experiment in such a way that the zero crossings in the calculated $\mathrm{Re}[\epsilon(\omega)]$ coincided with the experimental zero crossings. The shifts needed to accomplish this were 0.15 eV for the NR and 0.3 eV for the SR spectra. LDA calculated the band-gaps to be 0.99 and $\simeq 0$ eV in the NR and SR case, respectively, and these values should be compared to the experimental gap of 0.23 eV.[5] Therefore, we find, in agreement with earlier findings,[1] that there is no direct relation between the necessary shifts of the spectra, and the error in the calculated LDA band gaps. The improvement upon the calculated (shifted) dielectric function $\epsilon(\omega)$ after the inclusion of scalar relativistic effects in the ground-state DFT calculation is clear from Fig. 3. The overall agreement of the $\epsilon(\omega)$ with the inclusion of SR effects and experiment[22] is very good, even though there are still some features to be improved. For example, the position of the E_2 peak[23] (high-energy peak in $\mathrm{Im}[\epsilon(\omega)]$) coincides with experiment, but it is too sharp and the magnitude is overestimated compared to experiment. Although we do find the right magnitude for the E_1 peak (low-energy peak in $\mathrm{Im}[\epsilon(\omega)]$), the double peak structure found in experiment is not reproduced.

V. CONCLUSIONS

We show how to include scalar relativistic effect within the zeroth-order regular approximation in time-dependent density-functional theory for the optical response properties of nonmetallic crystals. These TDDFT equations can also be applied to calculate the optical response properties of semimetals, because they do not show any singular behavior even though the Kohn–Sham band gap vanishes. The band structure of InSb shows a considerable stabilization of the *s*-like conduction band minimum with the inclusion of SR effects in the ground-state DFT calculation. LDA predicts the band gap in the Γ point even to vanish, and therefore predicting InSb to be a semimetal. The relative error in the static value of the dielectric constant becomes 5% compared to experiment when SR effects are included in the ground-state DFT calculation as well as in the time-dependent response calculation. The same accuracy as was found earlier with our TDDFT implementation for the III-V compounds in the zinc-blende structure. The dielectric function with inclusion of SR effects is clearly an improvement over the NR one, and is quite good compared to experiment, although the spectral features are still somewhat shifted to too low energies compared to experiment.

APPENDIX: SMALL-FREQUENCY RESPONSE

As we argued before, it is instructive to investigate the $\mathbf{k}$-dependence of the off-diagonal $\hat{\mathbf{j}}$-matrix elements for the critical bands and region around Γ. Therefore, let us consider the following $\mathbf{k}\cdot\mathbf{p}$ analytic continuation of the Bloch, respectively, eigenfunctions near a special $\mathbf{k}$-point. The Bloch theorem allows for the following expansion:

$$\psi_{n\mathbf{k}+\mathbf{h}}(\mathbf{r}) = \exp(i\mathbf{h}\cdot\mathbf{r}) \sum_s c^s_{n\mathbf{k}}(\mathbf{h})\,\phi_{s\mathbf{k}}(\mathbf{r}), \tag{A1}$$

where the particular choice of eigenfunctions $\phi_{s\mathbf{k}}(\mathbf{r})$ constitutes a complete orthogonal basis at $\mathbf{k}$. In order to establish the orthogonality also for the $\psi_{n\mathbf{k}+\mathbf{h}}(\mathbf{r})$ functions the expansion coefficients have to satisfy

$$\sum_s c^{s*}_{n\mathbf{k}}(\mathbf{h}) c^s_{m\mathbf{k}}(\mathbf{h}) = \delta_{nm}\,. \tag{A2}$$

These coefficients can be found by substituting the expansion in the scalar relativistic Kohn–Sham equation and by calculating the inner products with respect to $\exp(i\mathbf{h}\cdot\mathbf{r})\psi_{s\mathbf{k}}(\mathbf{r})$. This yields the set of equations

$$\sum_t [\mathbf{h}\cdot\langle\phi_{s\mathbf{k}}|\hat{\mathbf{j}}|\phi_{t\mathbf{k}}\rangle + (\gamma_{s\mathbf{k}}h^2 - \epsilon_{n\mathbf{k}+\mathbf{h}} + \epsilon_{s\mathbf{k}})\delta_{st}] c^t_{n\mathbf{k}}(\mathbf{h}) = 0, \tag{A3}$$

in which the factor $\gamma_{s\mathbf{k}} = \langle\phi_{s\mathbf{k}}|\gamma(\mathbf{r})|\phi_{s\mathbf{k}}\rangle$, where we introduced the shorthand notation $\gamma(\mathbf{r}) = c^2/(2c^2 - v_{\mathrm{eff}}(\mathbf{r}))$. In the limit of $h \to 0$ the expression reduces to the simple relation $(\epsilon_{s\mathbf{k}} - \epsilon_{n\mathbf{k}}) c^s_{n\mathbf{k}}(\mathbf{0}) = 0$. Thus the coefficients $c^s_{n\mathbf{k}}(\mathbf{h})$ have to vanish asymptotically unless $\epsilon_{s\mathbf{k}} = \epsilon_{n\mathbf{k}}$ and hence they constitute an ordinary unitary transformation that mixes merely

degenerate states. Using these relations we can now evaluate the analytic continuation of the (vertical) $\hat{\mathbf{j}}$-matrix elements near $\mathbf{k}$. First consider

$$\langle \psi_{n\mathbf{k}+\mathbf{h}} | -i\gamma(\mathbf{r})\nabla | \psi_{m\mathbf{k}+\mathbf{h}} \rangle = \sum_{s,t} c^{s*}_{n\mathbf{k}}(\mathbf{h}) \langle \phi_{s\mathbf{k}} | \gamma(\mathbf{r})(\mathbf{h}-i\nabla) | \phi_{t\mathbf{k}} \rangle c^{t}_{m\mathbf{k}}(\mathbf{h}). \tag{A4}$$

The current matrices follow directly by adding the Hermitian adjoint to this expression. Note that $\gamma(\mathbf{r})=c^2/(2c^2-v_{\text{eff}}(\mathbf{r}))$ involves only the fully symmetric ground-state potential. The orthogonality of degenerate $\phi_{s\mathbf{k}}(\mathbf{r})$ eigenfunctions is due to symmetry, which is not affected by this totally symmetric factor. The orthogonality involving nondegenerate states with $\epsilon_{s\mathbf{k}} \neq \epsilon_{n\mathbf{k}}$ can be affected, but here the expansion coefficients behave asymptotically as $c^{s}_{n\mathbf{k}}(\mathbf{h}) \propto h$, i.e., they vanish in zeroth order as argued above. Since the factor $\gamma_{s\mathbf{k}}=\langle \phi_{s\mathbf{k}} | \gamma(\mathbf{r}) | \phi_{s\mathbf{k}} \rangle$ is identical for each partner of the set of degenerate states $\epsilon_{s\mathbf{k}}=\epsilon_{n\mathbf{k}}$, we can apply Eq. (A2) and thus get

$$\mathbf{j}_{nm}(\mathbf{k}+\mathbf{h}) = 2\gamma_{n\mathbf{k}}\delta_{nm}\mathbf{h} + \mathcal{O}(h^2) + \sum_{s,t} c^{s*}_{n\mathbf{k}}(\mathbf{h}) \langle \phi_{s\mathbf{k}} | \hat{\mathbf{j}} | \phi_{t\mathbf{k}} \rangle c^{t}_{m\mathbf{k}}(\mathbf{h}). \tag{A5}$$

By taking the derivative with respect to $\mathbf{h}$ of the $\mathbf{k}\cdot\mathbf{p}$ Eq. (A3), one can readily deduce that

$$\sum_{s,t} c^{s*}_{n\mathbf{k}}(\mathbf{h}) \langle \phi_{s\mathbf{k}} | \hat{\mathbf{j}} | \phi_{t\mathbf{k}} \rangle c^{t}_{m\mathbf{k}}(\mathbf{h}) = [\nabla_{\mathbf{h}}\epsilon_{n\mathbf{k}+\mathbf{h}} - 2\gamma_{n\mathbf{k}}\mathbf{h}]\delta_{nm} + [\epsilon_{n\mathbf{k}+\mathbf{h}} - \epsilon_{m\mathbf{k}+\mathbf{h}}] \sum_{s} c^{s*}_{n\mathbf{k}}(\mathbf{h}) \nabla_{\mathbf{h}} c^{s}_{m\mathbf{k}}(\mathbf{h}). \tag{A6}$$

In the limit $h \to 0$ we thus get for the diagonal terms $n=m$,

$$\nabla_{\mathbf{k}}\epsilon_{n\mathbf{k}} = \sum_{s,t} c^{s*}_{n\mathbf{k}}(\mathbf{0}) \langle \phi_{s\mathbf{k}} | \hat{\mathbf{j}} | \phi_{t\mathbf{k}} \rangle c^{t}_{n\mathbf{k}}(\mathbf{0}) = \langle \psi_{n\mathbf{k}} | \hat{\mathbf{j}} | \psi_{n\mathbf{k}} \rangle, \tag{A7}$$

a well-known result. In this particular case, i.e., for the critical states $\epsilon_{s\mathbf{k}}=\epsilon_{t\mathbf{k}}=\epsilon_{\text{Fermi}}$ at $\mathbf{k}=\Gamma$, all diagonal $\hat{\mathbf{j}}$-matrix elements vanish due to symmetry, so that we get a quadratic energy dispersion relation $\epsilon_{n\mathbf{k}}-\epsilon_{n\mathbf{0}} \propto k^2$. The leading order terms are then given by

$$\mathbf{j}_{nm}(\mathbf{k}) \approx \mathcal{O}(k)\,\delta_{nm} + \mathcal{O}(k^2), \tag{A8}$$

so we get a quadratic leading order in the off-diagonal $\hat{\mathbf{j}}$-matrix elements in the case of $\epsilon_{n\mathbf{k}}=\epsilon_{m\mathbf{k}}=\epsilon_{\text{Fermi}}$ with $n \neq m$.

In the subsequent analysis we can neglect any anisotropy in the energy dispersion, as well as the angular dependence of the $\hat{\mathbf{j}}$-matrix elements, without invalidating the arguments. In the evaluation of the small frequency behavior of the critical contributions to the various response kernels $\chi_{ab}(\omega)$, we encounter integrals of the following general form:

$$\Delta\chi_{ab}(\omega) \propto \int_{\Omega} \frac{(a_n(\mathbf{k}) + (-1)^n a^*_n(\mathbf{k}))k^{2n}}{k^2 - \omega + i\eta} d\mathbf{k} + \text{c.c.}(-\omega), \tag{A9}$$

where Ω is a small sphere surrounding Γ and n is the number of times the off-diagonal $\hat{\mathbf{j}}$-matrix elements appear in the numerator, i.e., $n=0$ for $\chi_{\rho\rho}(\omega)$, $n=1$ for $\chi_{\rho\mathbf{j}}, \chi_{\mathbf{j}\rho}(\omega)$, and $n=2$ for $\chi_{\mathbf{jj}}(\omega)$. Note that the diagonal elements do not contribute at all. The functions $a_n(\mathbf{k}) \approx a_n(\mathbf{0}) + \mathcal{O}(k)$ are regular functions of $\mathbf{k}$. The contributions of $\psi_{n\mathbf{k}}$ and $\psi_{n-\mathbf{k}} = \psi^*_{n\mathbf{k}}$ are related due to time-reversal symmetry, which has been made explicit in the combination of $a_n(\mathbf{k})$ and $a^*_n(\mathbf{k})$ in the numerator. These integrals can be evaluated directly, with a general structure given by

$$\Delta\chi_{ab}(\omega) \propto p_n(\omega) + \omega^n \sqrt{|\omega|} \cdot [q(\omega) - 2i\pi^2\theta(\omega)] + \mathcal{O}(h^{n+2}), \tag{A10}$$

in which the polynomial part $p_n(\omega)$ of order n contains only even(odd) powers of ω for even(odd) n, just like the regular contributions to the response functions which result from the nondegenerate bands. The additional terms [in which $\theta(\omega)$ is the unit step function and $q(\omega)$ a regular function of ω] scale like $\omega^n\sqrt{|\omega|}$ which is just one-half an order higher. We can conclude that the absence of a band gap does not lead to irregular contributions to the response functions, and that we can expect a small frequency behavior of $\chi_e(\omega) \approx \chi_e(0) + \mathcal{O}(\sqrt{\omega})$.

[1] F. Kootstra, P. L. de Boeij, and J. G. Snijders, Phys. Rev. B **62**, 7071 (2000).
[2] F. Kootstra, P. L. de Boeij, and J. G. Snijders, J. Chem. Phys. **112**, 6517 (2000).
[3] E. Burstein, H. Brodsky, and G. Lucousky, Int. J. Quantum Chem. **1**, 756 (1967).
[4] *CRC Handbook of Chemistry and Physics*, 80th ed. (CRC, Boca Raton, 1999).
[5] N. W. Ashcroft and N. D. Mermin, *Solid State Physics* (Holt, Rinehart, and Winston, New York, 1976).
[6] M. Cardona, N. E. Christensen, and G. Fasol, Phys. Rev. B **38**, 1806 (1988).
[7] G. Y. Guo, J. Crain, P. Blaha, and W. M. Temmerman, Phys. Rev. B **47**, 4841 (1993).
[8] E. van Lenthe, E. J. Baerends, and J. G. Snijders, J. Chem. Phys. **101**, 9783 (1994).
[9] E. van Lenthe, R. van Leeuwen, E. J. Baerends, and J. G. Snijders, Int. J. Quantum Chem. **57**, 281 (1996).
[10] P. H. T. Philipsen, E. van Lenthe, J. G. Snijders, and E. J. Baerends, Phys. Rev. B **56**, 13556 (1997).
[11] G. te Velde and E. J. Baerends, Phys. Rev. B **44**, 7888 (1991); J. Comput. Phys. **99**, 84 (1992).
[12] C. Fonseca Guerra, O. Visser, J. G. Snijders, G. te Velde, and E. J. Baerends, in *Methods and Techniques in Computational Chemistry*, edited by E. Clementi and G. Corongiu (STEF, Gagliary, 1995), p. 305.
[13] G. te Velde, Ph.D. thesis, Free University, Amsterdam, 1990.
[14] E. J. Baerends, D. E. Ellis, and P. Ros, Chem. Phys. **2**, 41 (1973).
[15] G. Wiesenekker, G. te Velde, and E. J. Baerends, J. Phys. C **21**, 4263 (1988).
[16] G. Wiesenekker and E. J. Baerends, J. Phys.: Condens. Matter **3**, 6721 (1991).

[17] F. Bassani and G. Pastori Parravicini, in *Electronic States and Optical Properties of Solids*, edited by R. A. Ballinger (Pergamon, Oxford, 1975).
[18] R. K. Willardson and A. C. Beer, *Semiconductors and Semimetals* (Academic, New York, 1966).
[19] A. Svane and E. Antoncik, J. Phys. C **20**, 2683 (1987).
[20] L. Leij, R. A. Pollak, F. R. McFeely, S. P. Kowalczyk, and D. A. Shirley, Phys. Rev. B **9**, 600 (1974).
[21] M. Z. Huang and W. Y. Ching, Phys. Rev. B **47**, 9449 (1993).
[22] P. E. Aspnes and A. A. Studna, Phys. Rev. B **27**, 985 (1983).
[23] Cf. nomenclature, e.g., M. Cardona, *Modulation Spectroscopy* (Academic, New York, 1969).